

EARTHQUAKE SIZE DISTRIBUTION: POWER-LAW WITH EXPONENT $\beta \equiv \frac{1}{2}$?

Yan Y. Kagan

Department of Earth and Space Sciences, University of California,

Los Angeles, California 90095-1567, USA;

Emails: ykagan@ucla.edu, kagan@moho.ess.ucla.edu

Abstract. We propose that the widely observed and universal Gutenberg-Richter relation is a mathematical consequence of the critical branching nature of earthquake process in a brittle fracture environment. These arguments, though preliminary, are confirmed by recent investigations of the seismic moment distribution in global earthquake catalogs and by the results on the distribution in crystals of dislocation avalanche sizes. We consider possible systematic and random errors in determining earthquake size, especially its seismic moment. These effects increase the estimate of the parameter β of the power-law distribution of earthquake sizes. In particular, we find that estimated β -values may be inflated by 1-3% because relative moment uncertainties decrease with increasing earthquake size. Moreover, earthquake clustering greatly influences the β -parameter. If clusters (aftershock sequences) are taken as the entity to be studied, then the exponent value for their size distribution would decrease by 5-10%. The complexity of any earthquake source also inflates the estimated β -value by at least 3-7%. The centroid depth distribution also should influence the β -value, an approximate calculation suggests that the exponent value may be increased by 2-6%. Taking all these effects into account, we propose that the recently obtained β -value of 0.63 could be reduced to about 0.52–0.56: near the universal constant value (1/2) predicted by theoretical arguments. We also consider possible consequences of the universal β -value

and its relevance for theoretical and practical understanding of earthquake occurrence in various tectonic and Earth structure environments. Using comparative crystal deformation results may help us understand the generation of seismic tremors and slow earthquakes and illuminate the transition from brittle fracture to plastic flow.

Short running title: EARTHQUAKE SIZE DISTRIBUTION

Key words: Gutenberg-Richter relation; Corner moment; Tapered Pareto distribution; Scalar and tensor seismic moment; Universality of earthquake size distribution; Random walk; 3-D random rotation; Earthquake depth distribution; Seismic tremors; Transition from brittle to plastic deformation.

1 Introduction

Earthquake size distribution is usually described by the Gutenberg-Richter (G-R) magnitude-frequency relation (see Section 2.2). The G-R distribution can be transformed into the Pareto (power-law) distribution for a scalar seismic moment M with the exponent $\beta = b/1.5$, where b is the parameter of the G-R law.

Theoretical analysis of earthquake occurrence (Vere-Jones, 1976, 1977) suggests that, given its branching nature, the exponent β of earthquake size distribution should be identical to $1/2$. Properties of the critical branching process explain this result: the total number of events (individuals) in such a process asymptotically is distributed according to a power-law with exponent 0.5 (Otter, 1949; Harris, 1963, Ch. I.13). Such distributions, obtained by simulations, are shown as upper curves in Figs. 7 and 8 below.

The same values of power-law exponents are derived for percolation and self-organized criticality (SOC) processes in a high-dimensional space (see discussion by Kagan, 1991a,

p. 132). Similar values of exponents are obtained by theoretical arguments and simulations for dislocation avalanches in crystalline materials (Zaiser, 2006, and references therein).

However, almost all the β or b measurements in earthquake catalogs result in estimates larger than $\frac{1}{2}$ (or 0.75 for the b -value). These estimates exhibit large variations in different regions, tectonic zones, etc. A search of the ISI database (Thomson Reuters Scientific) indicates that over the last five years, more than three papers on the b -value or the G-R relation were published monthly. The similar rate of publications of the papers discussing the magnitude-frequency relation can be observed in the previous 20-30 years. In almost all articles the variation of the b -value is attributed to different tectonics, rock stress, etc.

The following reasons for variability in the measured b - and β -values can be proposed:

- 1. Inappropriate usage of magnitude scales other than moment magnitude: only the moment magnitude should be studied. Regular earthquake magnitudes have significant systematic and random errors (Kagan, 1999, 2003), making them inappropriate for rigorous statistical, quantitative investigation.

- 2. The maximum or corner moment M_c (see Section 2.2) needs careful consideration (Kagan, 1991a; 2002a; Bird and Kagan, 2004). If M_c close to the magnitude/moment threshold – that is, the smallest magnitude/moment above which the catalog can be considered to be complete – and the earthquake size distribution is approximated by a plain G-R distribution, the magnitude-frequency curve would shift downwards, and the b - or β -estimates would be strongly biased upwards. In such a case to avoid the bias it is necessary to apply a two-parameter relation, which includes the maximum or corner magnitude.

- 3. Mixing populations of earthquakes from tectonic settings that have different corner magnitudes: when earthquake populations with a varying corner moment M_c are placed in the study samples, a false increase in the β -values results. Mixing populations with different M_c may even yield a seemingly linear curve in a log-log plot, in such a case a two-parameter

approximation of the magnitude-frequency relation would fail to avoid bias. For example, due to a significant corner moment variability, Kagan (2002a, Table 5, Section 5.2.3) determined the β -values on the order 0.8-1.1 for mid-ocean earthquakes. Similarly and apparently for the same reason, excessively large b -values for oceanic earthquakes were obtained by Okal and Romanowicz (1994) and Schorlemmer *et al.* (2005).

- 4. Relative seismic moment errors increase with decreases in earthquake size, resulting in a spurious β increase.

- 5. The object of study should be earthquake sequences, not individual earthquakes: theoretical estimates, discussed above, are relevant for earthquake *sequences*, not individual events. Hence β -values need to be corrected for this effect.

- 6. An earthquake is a tensor; its size, as given in moment tensor solutions, is a tensor sum of earthquake subevents. If these subevents have different focal mechanisms, their tensor sum would be smaller than that for scalar moments of subevents. Thus, even if the number of elementary earthquake events were distributed according to the power-law with the exponent $\beta \equiv \frac{1}{2}$, the distribution of earthquake size, as represented by the tensor sum, may have a larger exponent value. This follows from stochastic complexity in the source. If, for example, a source consists of positive and negative random n subsources, its size would be proportional to \sqrt{n} : the size would be similar to that at the end of a Brownian random walk.

- 7. The corner moment M_c is likely to change significantly with the depth for shallow earthquakes (Kagan, 1999, Section 1; Kagan, 2002a). For shallow seismicity, earthquake populations with various depths are usually added up, thus β determinations are biased. Earthquake catalogs with only the hypocenter information cannot be used to investigate this effect because hypocenters are often located at a lower or upper depth boundary of a fault rupture zone. On the other hand, the degree of accuracy of centroid depths in moment

tensor catalogs is presently too low to study rigorously the M_c depth variation.

On the basis of statistical analysis of several earthquake catalogs and some theoretical observations, Kagan (1991a, pp. 129, 132-3) conjectured that the β -value is a universal constant (1/2). Three additional arguments can now be added to strengthen this hypothesis: (a) more careful measurements of the β parameter in modern earthquake catalogs (mainly the CMT catalog) suggest that the β is universal; (b) recent advances in space geodesy and quantitative plate tectonics allowed for detailed calculation of tectonic deformation rate. By comparing tectonic and seismic moment rates, we can calculate the upper bound, M_c , for earthquake moment distribution; and (c) investigation of dislocation avalanches in crystals indicated that their size distribution is a power-law whose exponent has a universal value.

Several previous investigations (Kagan, 1999; Bird and Kagan, 2004; Boettcher and Jordan, 2004) suggested that the β has a universal value on the order of 0.63–0.67. Moreover, statistical analysis of earthquake size distribution and comparison of seismic and tectonic deformation rates allowed us to evaluate the corner moment (M_c) value for several tectonic regions. We conclude that apparent change in the β -values is due mainly to M_c variability.

However, the β universality model can be challenged. One can argue that more careful measurements may reveal statistically significant variations in the β exponent. The aim here is to show that the β -value is a universal constant. We consider various systematic and random effects whose influence would confirm this conjecture.

Recent experimental and theoretical investigations have demonstrated that crystal plasticity is characterized by large intrinsic spatio-temporal fluctuations with scale-invariant characteristics. In other words, deformation proceeds through intermittent bursts with power-law size distributions (Zaiser, 2006; Dahmen *et al.*, 2009). In particular, Csikor *et al.* (2007), Dimiduk *et al.* (2006), Weiss and Marsan (2003) studied dislocation avalanches (micro- and nano-earthquakes) in ice and other crystals. They consistently obtain the power-

law size distribution with the probability density exponent close to 1.5. This would correspond to our exponent $1 + \beta$. The power-size distribution in a single ice crystal extends over six decades of magnitude (Miguel *et al.*, 2001).

Comparing these dislocation avalanche measurements with seismological observations leads to some problems. The most accurate measurements of earthquake size are for the seismic moment. Experimental laboratory observations provide the energy of acoustic emission bursts or strain step measurements. Zaiser (2006, pp. 212, 223) argues that both these measurements are approximately equivalent and yield similar values for the distribution density power-law exponent (1.5–1.6).

Earthquake energy has the same distribution as the seismic moment. Kanamori (1977) cites the following relation between energy released by earthquakes, E , and their magnitude, m : $\log_{10} E = 1.5 m + 11.8$. Because the moment and magnitudes have a similar dependence (Kagan, 2002a), the exponents for energy and moment power-law distributions should be identical.

Another problem of comparison is that obtained statistical distributions of dislocation avalanches are not processed by appropriate statistical techniques. Thus, the obtained values of the exponents may be biased. For example, Zaiser *et al.* (2008) use the least-square fit to calculate the exponent. Richeton *et al.* (2005) apply the Levenberg-Marquardt algorithm for this purpose. These methods are appropriate for fitting regression curves, but they are not the most statistically efficient techniques for a parameter evaluation in statistical distribution. They may yield biased estimates of an exponent parameter and its uncertainty (Vere-Jones, 1988; Clauset *et al.*, 2009).

In Section 2 below we briefly review the earthquake size distribution formulas and consider the results of the β -value evaluation. Section 3 discusses systematic and random effects in earthquake size determination (items 4-7 above). In Section 4 we summarize the results

for determining β and compare our conclusions with studies of dislocation avalanches in brittle and plastic crystalline solids. We also discuss possible consequences for interpreting geophysical observations of regular and slow earthquakes and seismic tremors in brittle crust and the upper mantle.

2 Catalog analysis and earthquake size distribution

Only shallow earthquakes (depth 0-70 km) will be investigated in this work, because more data is available on them. Additionally, the seismic efficiency coefficient, or proportion of tectonic deformation released by such events, is close to 1.0 (Bird and Kagan, 2004). Geometry of deep earthquake faults is much less known than that for shallow seismicity, and may be more complex. For deeper earth layers (depth > 70 km) only a small part (less than 5%) of tectonic motion is released by seismicity (Kagan, 1999; Frohlich and Wetzell, 2007). Therefore, earthquake rupture in a brittle crust would be better modeled by the critical branching process theory.

As mentioned in the Introduction, regular magnitude measurements are subject to many random and systematic errors (Kagan, 2003). Kagan (1999, pp. 557-8) studied correlation between b -value estimates based on m_b and M_S magnitudes and found that the correlation coefficient is low (0.1–0.2). These coefficient values seem to indicate that b -value variations are not caused by regional tectonic or physical factors. Therefore, we investigate earthquake size distribution here using only seismic moment tensor measurements. The most complete, extensive, and accurate catalog of tensor solutions is the CMT dataset (Kagan, 2003).

2.1 CMT earthquake catalog

We studied earthquake distributions and clustering for the global CMT catalog of moment tensor inversions compiled by the CMT group (Ekström *et al.*, 2005; Ekström, 2007). The present catalog contains more than 30,000 earthquake entries for the period 1977/1/1 to 2008/12/31. Earthquake size is characterized by a scalar seismic moment M . The moment magnitude can be calculated from the seismic moment (measured in Nm) value as

$$m_W = (2/3) \cdot \log_{10} M - 6.0. \quad (1)$$

The magnitude threshold for the 1977-2008 catalog is $m_t = 5.8$; for the 1982-2008 catalog it is $m_t = 5.6$ (Kagan, 2003). An earthquake catalog is considered reasonably complete at and above the magnitude threshold (or the corresponding seismic moment, Eq. 1). Since we use only the moment magnitude in this work, the subscript is usually omitted.

2.2 Seismic moment distribution

The distribution of earthquake size is usually described by the classical G-R (Gutenberg and Richter, 1944) magnitude-frequency relation

$$\log_{10} N(m) = a_t - b(m - m_t) \quad \text{for } m_t \leq m, \quad (2)$$

where $N(m)$ is the number of earthquakes with magnitude $\geq m$, and a_t and b are parameters: a_t is the logarithm of the number of earthquakes with $m \geq m_t$ (the seismic activity or earthquake productivity level) and b describes the relation between numbers of small and large earthquakes. The G-R laws seems to apply to earthquakes as small as $m = -1.3$ (Boettcher *et al.*, 2009), with a rupture length on the order of 0.5 m, and as large as the 2004 $m9.2$ Sumatra, with about a 1200 km rupture.

The G-R relation (2) can be transformed into the Pareto (power-law) distribution for the scalar seismic moment M . The distribution in a probability density form is (Kagan, 2002a)

$$f(M) = \beta M_t^\beta M^{-1-\beta} \quad \text{for } M_t \leq M; \quad (3)$$

in a survivor function (1 – cumulative distribution) form it is

$$F(M) = (M_t/M)^\beta \quad \text{for } M_t \leq M, \quad (4)$$

where β is the index parameter of the distribution, and $b = \frac{3}{2}\beta$.

The tapered G-R (TGR) relation has an exponential taper applied to the number of events with a large seismic moment. Its probability density function is

$$f(M) = \left[\beta + \frac{M}{M_c} \right] M_t^\beta M^{-1-\beta} \exp\left(-\frac{M_t - M}{M_c}\right) \quad \text{for } M_t \leq M < \infty. \quad (5)$$

Here M_c is the parameter controlling the distribution in the upper ranges of M ('the corner moment'). The survivor function is

$$F(M) = (M_t/M)^\beta \exp\left(-\frac{M_t - M}{M_c}\right) \quad \text{for } M_t \leq M < \infty. \quad (6)$$

Equations (5) and (6) are equivalent to (3) and (4), respectively, if $M_c \rightarrow \infty$.

Fig. 1 displays cumulative distribution (survivor function) for the scalar seismic moment of shallow earthquakes in the CMT catalog for 1977-2008. The curves display a scale-invariant (Pareto) segment (linear in the log-log plot) for small and moderate values of the moment magnitude m . But for large m , the curve clearly bends downward (see Fig. 2 by Kagan *et al.*, 2010 for comparison).

In a regular β estimation we construct a likelihood map in $[\beta \times m_c]$ space (Fig. 2) and find its maximum (compare Figs. 6 and 7 by Bird and Kagan, 2004, or Fig. 3 by Kagan *et al.*, 2010). The 95% confidence level corresponds to the contour value 0.0. Only the lower confidence limit for the corner magnitude $m_c \simeq 8.3$ can be determined. The upper limit is

not defined in the map. The tapered Pareto distribution with the parameters corresponding to the maximum likelihood function, is shown in Fig. 1 by the dashed line. Sometimes these maps exhibit a significant correlation between the estimates of parameters, see Figs. 6 G,H and 7 B,E by Bird and Kagan (2004), complicating M_c evaluation and application. Since our map does not display the interdependence between these two parameter estimates, simpler procedures for determining β can be used (Kagan, 2002a).

In Fig. 3 we show the normalized difference between the observed magnitude-frequency relation in Fig. 1 and its approximation by the tapered Pareto or the tapered Gutenberg-Richter (TGR) relation. We assume that the earthquake numbers in a frequency plot follow the Poisson distribution. Kagan (2010) demonstrates that the temporal distribution of large earthquakes approaches the Poisson law. Kagan *et al.*, (2010, Table 2) show that in the CMT catalog due to its high moment threshold the aftershock numbers are less than 25% of the total. For large number of events its standard deviation (σ) is a square root of the number. To normalize, we divide the difference by $1.96 \times \sigma$; hence the ± 1 ordinate value would correspond to the 95% confidence level.

Fig. 4 demonstrates a possible source of bias in determining magnitude: earthquakes of different size have their size estimated differently. The moment inversion in the CMT catalog is carried out using some combination of three types of waves: body, surface, and mantle waves (Dziewonski *et al.*, 1981; Dziewonski and Woodhouse, 1983; Ekström, 2007). The mantle low-frequency (period 135 s) waves are used mostly for larger earthquakes. Higher-frequency body and surface waves are used for more moderate events (see also Fig. 2 by Kagan, 2003). For shallow earthquakes, Fig. 4 shows the fraction of each wave used in the solution for each moment magnitude. Earthquake sizes are estimated by some combination of the different wave types, so the sum of three points in any given magnitude bin may exceed unity. For example, up to $m = 7.5$ almost 90% of earthquakes have body waves implemented

in the solution. After that the inversion is based mostly on mantle waves. Therefore, we may posit that the statistically significant deviation for the tapered Pareto distribution at $m > 7.8$ (see Fig. 3) may be caused by transition from the body- to mantle-wave estimate. It is possible, of course, that the change in both plots (Figs. 3 and 4) at about $m = 7.5$ is a coincidence. Presently we lack data to thoroughly test this hypothesis.

3 Systematic and random effects in determining earthquake size

This section considers in detail four sources of magnitude/moment bias mentioned in the Introduction (items 4-7).

3.1 Scalar seismic moment errors

There is a bias in evaluating the G-R parameters due to random errors in determining magnitude (Molchan and Podgaetskaya, 1973, p. 47, Eq. 7; Tinti and Mulargia, 1985, p. 1690). This magnitude error is assumed to be symmetric and Gaussian, the error analysis by Kagan (2003, see Figs. 12-15) seems to confirm this. Generally, as long as the moment or amplitude errors are relatively small, one should expect them to be Gaussian as they are the result of summing up many independent random uncertainties.

The magnitude error causes a shift of the a estimate in (2) toward larger values: given the approximate symmetry of the error distribution, more weak earthquakes have their magnitude increased than vice versa:

$$a_{\text{estim}} = a_{\text{corr}} + \frac{b^2 \sigma_m^2 \log 10}{2}, \quad (7)$$

where σ_m is a standard error in the magnitude estimate, a_{corr} is the corrected (true) a -value,

a_{estim} is the measured a -value. Otherwise, the bias may manifest as a right-hand (horizontal) magnitude shift in the G-R curve

$$m_{\text{corr}} = m_{\text{estim}} - \frac{b \sigma_m^2 \log 10}{2}, \quad (8)$$

where m_{corr} is the corrected magnitude, m_{estim} is the measured magnitude. For $b = 1$ the shift is of the same amplitude in (7) and (8).

If the magnitude errors do not depend on the magnitude, this error does not practically influence the estimated b -value (Tinti and Mulargia, 1985). However, if σ_m is a function of m , the b estimates would be affected by magnitude errors.

Rhoades (1996, 1997) derived the theoretical estimates of a bias in the b -value in such a case. Rhoades (1996) and Rhoades and Dowrick (2000) studied the influence of magnitude errors on b -value estimates and provided some approximate estimates for the b -bias from such errors. In these evaluations they assumed that magnitude errors increase as the magnitude itself increases: for the j -th measurement of magnitude $\sigma_j = 0.1 (1 + u_j m_j)$, where u_j is a random number uniformly distributed on the interval $[0, 1]$, the magnitude threshold is 3.95 and the real b -value is 1.0. They found that the ‘measured’ b -value decreases by about 4% compared to its true value.

The CMT catalog supplies inversion errors for tensor moment components (Dziewonski *et al.*, 1981; Dziewonski and Woodhouse, 1983). It is important to distinguish magnitude and moment random errors. Magnitude is defined as a logarithm of appropriately scaled and averaged amplitude (A) of specific seismic waves: $m = \log_{10} A + C$, where C is a coefficient. Therefore, for small amplitude uncertainties the standard error in the amplitude measurements (σ_A) is related to the magnitude error (σ_m) as

$$\sigma_m \propto \frac{\partial m}{\partial A} = \frac{\sigma_A}{A} \times C, \quad (9)$$

i.e., the magnitude error is proportional to a *relative* amplitude error. A similar relation is valid for the scalar seismic moment (see Eqs. 10 and 13 below).

Kagan (2002a) measured the scalar seismic moment errors in the CMT catalog and found that the relative moment errors actually *decrease* with the earthquake size, implying that the *magnitude* errors should also decrease. We define the relative moment error, ϵ , as the ratio of the error tensor norm to the moment tensor norm

$$\epsilon = \sqrt{\frac{\sum_{i,j} E_{ij}^2}{\sum_{i,j} M_{ij}^2}}, \quad (10)$$

where E_{ij} and M_{ij} are standard error and moment tensor components, respectively. The distribution of ϵ for the CMT catalog 1977-2008 is shown in Fig. 5 (compare Fig. 5 in Kagan, 2002a). Since the influence of the magnitude threshold value is insignificant for determining the relative moment error, we use $m_t = 5.6$ in this plot. We calculate two regression lines approximating the dependence of the errors on the magnitude: the linear and quadratic curves

$$\log_{10} \epsilon = c_0 + c_1 (m - 6) + c_2 (m - 6)^2. \quad (11)$$

We use $(m - 6)$ instead of m as an argument, so that the c_0 -value would have a clear intuitive meaning.

In the diagram (Fig. 5) the coefficient of correlation between ϵ and the magnitude is -0.47 , indicating that relative moment errors decrease with the increase of m . Residual regression errors are close for both linear and quadratic cases: $\sigma = 0.274$ and $\sigma = 0.267$, respectively. From the diagram it is clear that errors for earthquakes with $m > 6.5$ deviate significantly from a linear trend. However, since the number of strong earthquakes is small, the residuals of the linear and quadratic cases do not differ significantly.

The parameter values in (11) for two subsets of the CMT catalog are listed in Table 1.

The ϵ -values for earthquakes in the magnitude range 5.4–6.4 can be represented as

$$\epsilon \approx 0.056 \times 10^{-0.54(m-6)}, \quad (12)$$

for shallow events in the 1982-2008 CMT catalog (see Table 1). For small ϵ the magnitude error σ_m is calculated as

$$\sigma_m \approx \frac{\epsilon}{1.5 \log 10}. \quad (13)$$

Modifying (8) or Eq. 10 in Rhoades and Dowrick (2000), we obtain the following magnitude correction for the magnitude estimates perturbed by random errors:

$$m_{\text{corr}} = m_{\text{estim}} - \frac{3}{4} \sigma_m^2 \beta \log 10. \quad (14)$$

To apply this formula to b or β correction, we estimate σ_m at two magnitude values (5.4 and 6.4) and use (14) to compute $\delta_c m = m_{\text{corr}} - m_{\text{estim}}$. Performing such calculations for the relative moment error ϵ in (13), we obtain the correction for β of shallow earthquakes 0.0013: a β is decreased by about 0.2%.

However, our calculations could not consider one important source of error. For many weak shallow earthquakes in the CMT catalog, no solution can be obtained for the tensor components $M_{r\theta}$ and $M_{r\phi}$ (Dziewonski *et al.*, 1981, p. 2829; Dziewonski and Woodhouse, 1983; Frohlich and Davis, 1999). In such a case, $E_{r\theta}$ and $E_{r\phi}$ as well as $M_{r\theta}$ and $M_{r\phi}$ are set to zero. About 4% of shallow earthquakes have this problem (Kagan, 2003, pp. 195-196). For strike-slip events which predominate in this group, the tensor components $M_{r\theta}$ and $M_{r\phi}$ are close to zero. This means that if the values of E_{ij} and M_{ij} were available for these events in (10), the numerator value should be much greater, but the denominator would be essentially the same. This would significantly increase the resulting ϵ -value.

Moreover, apparently the relative moment error, ϵ , is only part of the total seismic moment error. Dziewonski *et al.* (1981) and Dziewonski and Woodhouse (1983) suggested

the standard errors obtained in the CMT solutions likely to be underestimated. Kagan (2000, 2002a) estimated that the reported errors are possibly 1/3 to 1/2 of the total. Because the bias in estimating β depends on the square of the magnitude estimation error (see Eq. 14), a systematic bias as high as 1-3% may be caused by the decrease of the relative magnitude uncertainty with the increasing earthquake size.

3.2 Earthquake sequences and their influence

As mentioned in the Introduction, theoretical β estimates should be only relevant for earthquake *sequences*, not individual events. We take that an earthquake belongs to sequences and sequences being the theoretical entity of interest, rather than individual earthquakes. Registration of aftershock sequences (Kagan, 2004; Enescu *et al.*, 2009) shows that immediate aftershocks observed in high-frequency seismograms are included in mainshock or large aftershocks in catalogs based on long period registration. Thus, for example, the CMT catalog earthquakes include some close aftershocks.

In our model earthquake sequences are produced by the same critical branching process. Later aftershocks are separated into individual events due to temporal delays controlled by Omori's law (Kagan and Knopoff, 1981). Occasionally, the first event in a sequence is weaker than the following events, in which case it is commonly called a 'foreshock' (*ibid*). Therefore, we could consider an earthquake cascade or foreshock-mainshock-aftershock sequence as one entity.

Here we attempt to study the seismic moment distribution for earthquake sequences. To define the sequences, we use the results of the likelihood analysis of earthquake catalogs (Kagan, 1991b). We approximate an earthquake occurrence by a multidimensional Poisson branching cluster process. In this model spontaneous events are distributed according to the Poisson distribution, whereas dependent events in earthquake sequences are controlled

by a distribution characterized by a few adjustable parameters. Each event, even if it is a member of a cluster, may start its own sequence, hence aftershocks may be of the first-, second-, third-, etc., order. The parameters of the model are estimated through a maximum likelihood search. A similar scheme has been proposed recently by Zhuang *et al.* (2002, 2004).

As the result of the likelihood optimization, we evaluate probabilities (p_{ij}) of any i -th earthquake belonging to a j -th cluster or sequence ($\sum_j p_{ij} = 1$); p_{ii} corresponds to the probability that an earthquake will be considered independent. We use these probabilities (p_{ij}) to assign a part of the seismic moment of the i -th event to the j -th earthquake; the j -th earthquake might again belong to some k -th group, etc. This process continues until all earthquakes and their interconnections in a catalog have been counted. In the end, some of the aftershock moments are transferred to their mainshocks if the aftershock probably belongs to the particular mainshock's cluster. As a result of this seismic moment reassignment, some earthquakes may have a seismic moment below the magnitude threshold, m_t . We remove these earthquakes from a catalog.

As the number of earthquake sequences is always smaller than the number of earthquakes in a catalog, while the total moment in a catalog is constant, we should expect the β -value for sequences to be smaller than that for individual earthquakes. For deep and intermediate earthquakes, the difference in the β -values in calculations which use sequences and those using individual earthquakes is negligible. This small difference is due to a small number of aftershocks for these sequences in the CMT catalog (Kagan, 1999, Table 4).

Generally, we can treat the probabilities of being independent (p_{ii}) as corresponding to the weight of an earthquake as it is included in calculations. However, to make our computations similar to those used for real catalogs, we simulate new catalogs leaving in only earthquakes whose p_{ii} exceeds a random number distributed uniformly in the [0-1] interval. Thus, we

obtain a ‘declustered’ catalog, in which we delete an earthquake according to its probability of being dependent.

Table 2 shows several β measurements for two CMT shallow earthquake subcatalogs, 1977-2008 and 1982-2008, with the magnitude threshold $m_t = 5.8$ and $m_t = 5.6$, respectively. For global datasets three types of computation were performed: (a) in the original list, (b) in a declustered catalog, where seismic moment has been preserved for each earthquake, and (c) in a declustered catalog with aftershock moment transferred to an appropriate mainshock according to probabilities p_{ij} (see above). We performed similar measurements for earthquakes in subduction zones (trenches) (Kagan *et al.*, 2010). Trench earthquakes have not been declustered, because some may have connections to outside events. Therefore the dependence probabilities can be biased.

In Table 2 the β -values are smaller by about 1-3% for the 1982-2008 dataset compared to the 1977-2008 catalog. Probably a higher average accuracy of these solutions (Kagan, 2003) and larger magnitude range explains this reduction. Bird and Kagan (2004) showed that for global seismicity the minimum value of m_c for some tectonic zones is of the order 5.9–6.6. Extending the magnitude threshold to $m_t = 5.6$ expands the power-law part of the plot, and the influence of the corner magnitude is smaller.

The β bias in the Table is also caused by the mix of different earthquake populations with various corner magnitudes, m_c (item 3 in the Introduction). This effect could explain why the β -values for trenches are significantly lower (by about 5%) than the global ones. A global earthquake set consists of many populations, of which oceanic rift zones have the smallest m_c -values (Bird and Kagan, 2004). These oceanic events are excluded from the subduction zone (trench) dataset. Hence, the estimate of β for trench earthquakes is closer to the theoretical value than for earthquakes in any other tectonic province.

As expected, the β -values decrease for the declustered catalogs, since excluded aftershocks

have smaller moment values. This reduction is even stronger for catalogs where the aftershock moment is assigned to their potential mainshocks. The β -value decreases are about 4.5% and 8.5%, respectively.

These bias estimates depend on the correctness of the calculations used to estimate earthquake probabilities. The likelihood procedure used to assign the probability of event independence is influenced by catalog quality, length and magnitude threshold. Given the presence of temporal boundaries, many relations between earthquakes are missed: some events of the beginning of the catalog may be aftershocks of previous strong quakes. Thus, instead of having a probability closer to zero, as they should, these aftershocks would have an independence probability equal to 1.0.

Due to the magnitude threshold, some connections between events are not observable. Suppose there is a potential foreshock-mainshock pair: a larger earthquake is preceded by a smaller one. However, the first event is below the magnitude threshold and the larger quake is above it. Then this second event would be treated as independent; our calculations would not include this connection (Kagan, 1991b).

Moreover, the likelihood model used in our inversion is not perfect (Kagan, 1991b). As a result, the independence probability values of earthquakes may not be fully counted leading to a bias in the β computations. Therefore, the reduction of the β -values due to the influence of aftershock sequences is likely to be greater.

If we add up all the influences of aftershocks, we should see the β -value decrease to about 0.59–0.6. Kagan (1991a, p. 129) and Kagan (1999, Table 5) obtained a similar result for declustered shallow earthquakes.

3.3 Seismic moment tensor and its complexity

The previous discussion assumed that scalar seismic moment is a fair measure of earthquake size. In reality seismograms are caused by excitation from many subevents during the main phase of an earthquake. Thus, the seismic moment tensor of an earthquake is a compound tensor sum of subevents. If all these subevents were identically oriented, the tensor sum would be proportional to a scalar sum of all the subevent scalar moments. However, detailed studies of earthquakes clearly indicate that subevent orientation changes significantly during ruptures.

The Bulletin of the Seismological Society of America (BSSA) published several special issues dedicated to thorough analysis of several large earthquakes like the 1992 Landers, 1999 Hector Mine, the 1999 Chi-Chi, Taiwan, the 2002 Denali, the 2004 Sumatra, and so on. These studies detail a very complex geometrical picture of the quake rupture process. The focal planes and slip vectors of earthquake subevents often rotate several degrees and even tens of degrees. Therefore, the seismic moment tensor solution and the resulting estimate of an earthquake scalar moment is subject to random fluctuations from the stochastic misalignment of earthquake components.

In principle, we could avoid the systematic effect caused by source complexity if we used an earthquake's energy as a measure of its size. Energy is a positive scalar; thus, no bias due to source complexity would appear in the energy estimate. Unfortunately, estimates of the radiated seismic energy are highly uncertain and often differ by up to an order of magnitude (Perez-Campos *et al.*, 2003). In contrast, the relative accuracy of evaluating seismic moment tensor is on the order of $10^{0.15}$ (Kagan, 2003).

Scalar moment earthquake estimates should always be lower than the sum of the subevents' scalar moments. This occurs because of random fluctuations during earthquake

fracture. This effect would also bias upwards the estimated β -values. Because we lack a comprehensive model of the earthquake rupture process which would enable us to estimate rigorously the resulting bias, we proceed by studying several approximations. These will give insight into the problem and provide an order of the magnitude estimate of possible systematic effects due to source complexity.

We can estimate the influence of source complexity on the resulting estimate of earthquake size by initially assuming that small elementary subevents have their sign selected randomly. If the sign changes with equal probability ($p = 0.5$), the resulting sum of the subevents would be an ordinary random walk. The walk would converge to Brownian motion if the number of subevents, n , is large. The sum would be distributed according to the Gaussian distribution with the standard deviation proportional to \sqrt{n} . The final value of the sum would be proportional to its standard error. (In a count of the Brownian sum, we use an absolute value of the final walk position. Therefore, the total ‘moment’ estimate is positive.) Therefore, in a critical branching process in which descendants are added with the random probability $p = 0.5$, the power-law index would increase by a factor of two: $\beta = 1.0$.

If we change the probability value from 0.5 to a higher level, $p = 0.5 + \delta$, this would produce Brownian motion with a drift (Feller, 1966). For small n values, the walk behavior would resemble a regular Brownian motion, and later the sum would have a steady component $n\delta$. Thus, its behavior would be similar to the cumulative number increase with $p = 1$.

Fig. 6 shows three simulated source-time functions with the time delay controlled by the Omori-type function. The cumulative functions for each curve are the sums of elementary subevents of the unit size and only the signs are different. The first with $p = 1$ (deterministic addition of events) is similar to Fig. 3 by Kagan and Knopoff (1981). The initial step-like increase of this function would likely be interpreted as a mainshock, whereas a few steps at

a later time would be labeled as aftershocks. The $p = 0.75$ function increases the same way as the first curve but with smaller amplitude; random fluctuations are not easily observable. The random walk function ($p = 0.5$) behaves more erratically and its total final ordinate is much smaller than that of the other two curves. Only the values of the curves at the end of a branching simulation, corresponding to the total moment of a sequence, are counted in our calculations. For the p -values close to 0.5, the random branching walk could end up as a negative cumulative sum; as we explained above, we take the absolute value of the final ordinate of a simulation run. These values are assumed to correspond to the total seismic moment of an aftershock sequence.

Fig. 7 illustrates the above considerations. We simulated a critical branching process and counted the sum of events at the end of each simulation run, such as the extreme right-hand points of three curves in Fig. 6. These numbers are shown in the diagram in the log-log format. While the event numbers are small (less than 10), the discretization effects are noticeable. For the largest sequences, random fluctuations are observable, because there are few of these sequences. In the mid-number range, the deterministic number addition ($p = 1$) distribution (red solid curve) has an index $\beta = 0.5$. As expected, the Brownian walk addition (blue dashed curve) has $\beta = 1.0$. As explained above, the curves for the motion with a drift first follow the Brownian curve; then they are parallel to the red curve. Thus, in the beginning their index is $\beta = 1.0$, and for larger numbers it changes to $\beta = 0.5$ confirming our predictions. The randomness in the number addition significantly increases the power-law distribution index.

In Fig. 8 we show a more complicated test. In a critical branching process simulation, we sum up seismic moment tensors instead of scalar quantities. In each simulation run, we determine a norm of the total tensor sum which for the seismic moment tensor is equivalent to the scalar moment. Again the red solid curve shows the distribution when the tensors

are identical. For other curves the tensors are independently randomly rotated through the 3-D rotation angle, Φ (Kagan, 2003, 2009). The maximum angle for a double-couple focal mechanism is 120° ; therefore, these tensors are rotated in a uniformly random manner. The angle $\Phi = 0^\circ$ corresponds to the zero rotation (red curve). If $\Phi < 120^\circ$, then the rotation is restricted, being uniformly random only for angles smaller than Φ .

The Fig. 8 diagram appears similar to the previous plot (Fig. 7). If the tensors' orientation is identical, power-law exponent $\beta = 0.5$. For a completely random orientation, $\beta = 1.0$, and for a restricted misalignment, the curves follow the latter distribution first and are then parallel to the former line.

As discussed earlier, many earthquake ruptures exhibit significant variations in focal mechanisms. However, detailed analyses of individual earthquakes are still rare and insufficient for rigorous statistical study. Therefore, we study the degree of misalignment in several mainshock/aftershock sequences. Kagan (2000) investigated the correlation of earthquake focal mechanisms and showed that the degree of mechanism 3-D rotation increases between earthquakes with temporal and spatial differences. Hence, we hope that immediate aftershocks of strong earthquakes will characterize the geometric complexity of their rupture process.

To this end we studied all shallow (depth 0-70 km) earthquakes in the 1977-2008 CMT catalog with a magnitude $m_1 = 7.5$ and higher. All earthquakes ($m \geq 5.6$) are considered aftershocks within the first 7 days of $m7.5$ earthquake occurrence and closer than

$$r = 75 \times 10^{(m_1 - 7.5)/2} \text{ km}, \quad (15)$$

(Kagan, 2002b) There are 105 mainshocks in the catalog and 81 of them have one or more aftershocks.

To investigate the orientation differences between a mainshock and its aftershocks, we

calculate the correlation invariant or tensor dot-product J_3 (Kagan, 1992; 2009)

$$J_3 = \sum_{i,j} m_{ij} n_{ij}, \quad (16)$$

for the main event (m_{ij}) and the sum of normalized tensors for the whole 7-days aftershock sequence (n_{ij}). Summation of repeating indices is assumed. Both m_{ij} and n_{ij} are normalized. In (16) $J_3 = 2.0$ means that focal mechanisms are identical; $J_3 = -2.0$ corresponds to components of both tensors having the opposite sign.

A J_3 histogram in Fig. 9 displays the correlation between tensors. Most correlation invariant values are close to 1.5–2.0. Thus, the aftershock focal mechanisms are similar to that of their mainshock. However, some J_3 -values are close to zero, and one is negative, testifying to a significant variation in the rupture process. The smallest J_3 -value is due to the November 2000 New Ireland earthquake sequence. The sequence started with a $m_W = 8.0$ left-lateral main shock on 16 November and was followed by a series of aftershocks with thrust mechanisms primarily (Geist and Parsons, 2005; Park and Mori, 2007). The negative J_3 -value signifies that the aftershocks have on average a slightly opposite orientation to their mainshock.

Fig. 10 displays two distributions of the ratio for the tensor sum of the mainshock and its aftershocks to the sum of their scalar moments

$$R = |\sum m_{ij}| / \sum M, \quad (17)$$

where $|m_{ij}|$ means the norm of the tensor. The aftershocks are selected according to the same criteria as in Fig. 9. If aftershocks have the same focal mechanism as the mainshock, the ratio would be 1.0. In the left diagram of Fig. 10 the moment tensors are not normalized; in the right plot they are. In the inversions of the earthquake rupture process (see the BSSA special issues mentioned above), several subevents of approximately equal size but

significantly different orientation in focal mechanism are often observed. This is the reason we investigate the normalized sums.

The diagrams show significantly varied focal mechanisms in aftershock sequences. Large fluctuations are seen in the normalized sums especially. This result suggests again a conspicuous randomness occurs in the focal mechanism orientation of earthquake sequences. By implication this should also occur during an earthquake rupture process. Such random fluctuations may noticeably decrease the measured earthquake size and influence the β measurement.

What is the size of the β measurement bias? All estimates shown above are indirect. Earthquake do not consist of an identically oriented or purely random collection of elementary sources. Various observations suggest that a rupture occurs over quasi-planar fault patches, so there will be a strong correlation between neighboring fault segments. This correlation is sometimes broken by significant fault branching. Kagan (1982) proposed a geometrical model of such stochastic rupture. Unfortunately, the degree of geometrical branching (ϕ_0) in this model is not well known for different tectonic provinces. Therefore, we cannot easily simulate and study such branching sequences.

What β -value change can be proposed as randomness result in the fault rupture orientation? Pure randomness yields β -value increase by a factor of two (see Figs. 7 and 8). Unfortunately, we cannot yet quantitatively study the complex geometry of earthquake rupture. We need to extrapolate from the measured misalignments of close aftershocks. These measurements indicate that complexity, though far from being completely random, is nevertheless quite significant. For example, in Fig. 9 the correlation invariant is $J_3 = 1.46 \pm 0.55$. These values can be compared to purely random arrangements of double-couple focal mechanisms (Kagan, 1992), where $J_3 = 0 \pm 0.89$ has been obtained.

The frequency plot for randomly oriented double-couples obtained by simulation is shown

in Fig. 11. As expected, the histogram curve is symmetric around $J_3 = 0$ and reaches the maximum at $\text{abs}(J_3) = 1$. It would be interesting to obtain an analytical solution for J_3 , as we did for the 3-D rotation angle (Kagan, 2009). This can be done in the future.

If focal mechanisms are all parallel, $J_3 = 2.0$ (see more in Kagan, 2009). Therefore, we can make a rough guess that the degree of the β -value increase would be on the order of 10-15%, when extrapolated to a time close to zero: during the mainshock rupture. This guess is obtained by comparing the average J_3 shift in Fig. 9 ($\overline{J_3} - 2.0 = 0.542$) with that for the completely random arrangement in Fig. 11 ($\overline{J_3} - 2.0 = 0.0$), and by comparing standard deviations for both cases: 0.55 and 0.89, respectively.

Similar conclusions could be inferred from the results of the 3-D rotation angle distribution. The average angle between the mainshock focal mechanism and mechanisms of immediate aftershocks is on the order of 10° (Kagan, 2000). For a completely random rotation, the maximum angle is 120° and the average angle is 75.2° (Kagan, 2003). Given the source complexity, as demonstrated by the rotation angles, the β bias should be around 8-12%.

Analogous conclusions could be drawn from Fig. 10. If immediate aftershocks had the same moment tensor solutions as their mainshock, the tensor/scalar sum ratio R in (17) should be 1.0, and $(1 - R)$ equal zero. Both average and standard deviation for $(1 - R)$ in the plots display significant non-zero values. We infer that the source is complex and the β bias may be on the order of few percent.

To summarize the results of this subsection, we hypothesize that as a consequence of the random geometrical misalignment of a fault rupture, the measured β -value may be increased by at least a few percent (3-7%) from its true size. The estimate above is conservative. More work needs to be done to obtain a more reliable value which could lead to an even greater β -estimate decrease.

3.4 Centroid depth influence

The CMT catalog supplies earthquake coordinates for the seismic moment centroid (Dziewonski *et al.*, 1981; 1983); the centroid is in the center of the moment release volume. The centroid distance from the fault edge cannot be smaller than a half of the earthquake rupture zone width. Closer to the surface or to the fault boundary the corner moment would approach zero. An inspection of seismic maps suggests that hypocenters of larger events are on average deeper than those for small earthquakes. Thus, the moment-frequency law (see Eqs. 5 and 6) would change due to an increase of the maximum earthquake size with depth (Kagan, 2002a, p. 539). Therefore the corner moment for deeper earthquakes would increase.

As we explained in the Introduction, the depth accuracy for shallow earthquakes is presently insufficient to investigate observationally the dependence of the corner moment on depth. Therefore, we study a possible influence of the finite fault size by calculating a new distribution of earthquake size for a few simple models of the earthquake rupture pattern. These theoretical guesses would help evaluate the depth effect up to the order of magnitude.

We assume that earthquakes are distributed over an infinite planar fault surface extending either vertically for 20 km (imitating conditions for strike-slip faults in California), or distributed over an inclined fault with a width of 200 km (as in some subduction zones, see, for instance, Bird and Kagan, 2004). The variable corner moment for such faults is

$$M'_c = C \zeta^3, \tag{18}$$

where ζ is distance from a centroid to a fault edge and C is an appropriate coefficient.

In one model we assume that earthquake centroids are distributed uniformly over the fault surface. Then, using the algebraic and numerical facilities of `MATHEMATICA` (Wolfram,

1999), we calculate the new survivor function

$$\Psi_1(M) \propto \int_0^L F(M) d\zeta = \left(\frac{M_t}{M}\right)^\beta \int_0^L \exp\left(\frac{M_t - M}{C \zeta^3}\right) d\zeta = \left(\frac{M_t}{M}\right)^\beta \frac{\Gamma\left(-\frac{1}{3}, \frac{M-M_t}{C L^3}\right)}{3\left(\frac{C}{M-M_t}\right)^{1/3}}, \quad (19)$$

where $F(M)$ is defined by (6), L is a half-width of a fault plane, and $\Gamma(\cdot, \cdot)$ is an incomplete gamma function (Abramowitz and Stegun, 1972, Eq. 6.5.3).

The other possibility is to assume that earthquake centroid density increases linearly with increasing depth up to the middle of the fault width. The density decreases to zero thereafter. Kagan (2007, Fig. 6) shows that such a feature is a common occurrence. Then the survivor function would be

$$\Psi_2(M) \propto \int_0^L F(M) \zeta d\zeta = \left(\frac{M_t}{M}\right)^\beta \int_0^L \exp\left(\frac{M_t - M}{C \zeta^3}\right) \zeta d\zeta = \left(\frac{M_t}{M}\right)^\beta \frac{\Gamma\left(-\frac{2}{3}, \frac{M-M_t}{C L^3}\right)}{3\left(\frac{C}{M-M_t}\right)^{2/3}}. \quad (20)$$

Fig. 12 displays two survivor functions corresponding to Eqs. 6 and 20. In a loglog plot the former function has a linear part for the moment M values that are significantly smaller than the corner moment M_c . We take a slope β to be 0.5. The curve has an exponential taper for M close to M_c . On the other hand, the latter function (20) is slightly convex even for small moment values. It is formed by a sum of distributions similar to (6) but with the corner moment increasing from zero to the maximum, M_c . Therefore, we can only calculate an effective slope (β') of the curve; for the moment range 10^{17} – 10^{19} Nm, the slope β' in the plot is 0.523.

We calculate three theoretical curves for both equations (19 and 20): (a) fault width $L = 200$ km and $M_c = 10^{23}$ Nm ($m_c = 9.33$); (b) $L = 200$ km and $M_c = 10^{22}$ Nm ($m_c = 8.67$); and (c) $L = 20$ km and $M_c = 10^{21}$ Nm ($m_c = 8.0$). For the formula (19) the β' -values are 1.3, 2.8, and 6.6% higher than the original β -value, for the second formula these exponent increases are reduced by a factor of 1.4.

4 Discussion

In the previous sections we analyzed the index of the power-law distribution for earthquake size (the β -value) to argue that its true value is $1/2$, the value suggested by theoretical arguments. The direct β measurements for scalar seismic moment based on catalog analyses (Kagan, 1999; Bird and Kagan, 2004) usually yield a value in the range 0.63–0.67, equivalent to the commonly known G-R b -value of 0.95–1.0. Four systematic and random factors that bias the β -value estimate upwards are investigated: dependence of errors on the magnitude, earthquake sequences, complexity of earthquake source, and a finite size of earthquake faults (items 4-7 in the Introduction). We found that these factors would decrease the observational β -estimate by about 1–3%, 5–10%, 3–7%, and 2–6%, respectively. Of these values the third is most uncertain, because it is based on extrapolating immediate aftershock focal mechanisms to the mainshock’s rupture time.

If we combine the above biases and apply them to the most accurately determined β -value, i.e., β equals from 0.63 to 0.64 for subduction zones (Bird and Kagan, 2004), the corrected β -values would be on the order of 0.52–0.56. It is quite feasible that the second and third correction term are underestimated. This would imply that β is close to 0.5 and possibly equals $\frac{1}{2}$ exactly.

What theoretical conclusions could be drawn from this result? Solid state physicists explain new results on the scale-invariant distribution of dislocation avalanche size by suggesting a new theoretical approach to crystal plasticity (Zaiser, 2006). According to this interpretation, at a micro-scale the crystal deformation proceeds through intermittent bursts similar to earthquakes. Only at a larger, meso-scale does plastic deformation proceed as a smooth, homogeneous, quasi-laminar flow process. Crystal boundaries seem to influence this transition. In a single crystal the power-law distribution for energy of dislocation avalanches

is observed at the scale range of 10^6 . In polycrystal materials, the power-law distribution of bursts is also observed, but its size is limited by an upper cutoff.

Zaiser and Moretti (2005) and Csikor *et al.* (2007) propose the following probability density function for the dislocation avalanche energy or strain

$$P(s) = C s^{-\tau} \exp \left[-(s/s_0)^2 \right], \quad (21)$$

where C is a normalization constant, τ is a scaling exponent ($\tau \simeq 1.5$), and s_0 is the characteristic strain of the largest avalanches. This formula is similar to our (5) with exponent $\tau = 1 + \beta$, but the decay taper at large strain values is Gaussian like. We use instead the exponential decay. Because statistics on the largest events are insufficient in both cases, we cannot distinguish by observation between these formulas.

Therefore, plastic, ductile deformation proceeds by two very different mechanisms: (a) intermittent displacement at micro-scale with scale-invariant distribution of strain steps and the universal value of the power-law exponent ($\tau = 1.5$), and (b) in contrast a smooth flow at larger scales. Because detailed quantitative observation at small sub-grain scales was not possible until recently, the first mechanism had been largely ignored (Zaiser, 2006, p. 241).

The above considerations can be supported to some degree by recent analysis of earthquake size distribution. Bird and Kagan (2004) found that the exponent β of the power-law distribution appears universal in all eight tectonic provinces of global seismicity. In stark contrast, the corner moment differs by many orders of magnitude, from 10^{18} ($m_c = 6.0$) for oceanic normal faults to $10^{23.3}$ Nm ($m_c = 9.5$) for subduction zones.

Kagan (2002a, pp. 538-9) proposed that the observed b -value differences in volcanic areas, at creeping faults, and at the boundary between brittle crust and plastic deformation in the upper mantle may also be due to significantly varied corner moments. If earthquake populations with different m_c are mixed, the resulting statistical distribution could be interpreted

as belonging to a power-law with the exponent β significantly exceeding 0.6–0.7, the value normally observed in tectonic earthquakes.

Another geophysical phenomenon, the non-volcanic seismic tremor (Schwartz and Rokosky, 2007; Beroza and Ide, 2009, and references therein), may be explained by the same physical mechanism. The tremor represents long duration (minutes to hours) of a high-amplitude seismic signal, appearing similar to many small concatenated earthquake signals (Shelly *et al.*, 2007). The first observation of such non-volcanic tremors came during the aftershock sequence of the April 26, 1966 Tashkent (Uzbekistan) earthquake (Antsyferov *et al.*, 1971a, 1971b).

The tremor signals are sometimes quite pulsed in nature. For example, the temporal cumulative plot of seismic moment increase for tremors (Fig. 4d in Hiramatsu *et al.*, 2008) look similar to curves of crystal micro-deformation due to dislocation avalanches (Fig. 14 in Zaiser, 2006): both diagrams show that the displacement increases in discrete steps, each step is followed by a plateau.

Such tremors have been registered in diverse tectonic environments recently (Japan, Cascadia, New Zealand, Costa Rica, Taiwan, California). Tremor and other slow-slip events are typically found on the deep extension of faults, just below the region that produces the more familiar, ‘ordinary’ earthquakes. This recent observation of tremors has resulted in a flurry of research across many geologic and geophysical disciplines.

If tremors are a feature transitional between real earthquakes and seismic signal bursts, they are similar to the dislocation avalanches described above. Both phenomena occur in conversion from the brittle to plastic mode of solid deformation. Seismic tremors, which are interpreted as small, continually occurring earthquakes, may also have the same scale-invariant, power-law features as earthquakes in brittle crust. Hiramatsu *et al.* (2008) measured moment-frequency relation for tremors and found that it can be approximated by an

exponential distribution rather than a power-law. However, because of low signal-to-noise ratio for tremors, only the upper tail of tremor size distribution can be observed, and the upper tail for earthquake size distribution (see Eq. 5) is also exponential (Kagan, 2002a; Bird and Kagan, 2004). The higher end of the size distribution for dislocation avalanches also exhibits a non-power-law dependence (21) which is close to exponential law. We may conjecture that as with dislocation avalanches, the size distribution of smaller tremor events would be the power-law with the universal value of the exponent constant ($\beta = 0.5$). Further study of tremors should answer this question.

If we are correct about universality of the β -value constant ($\beta = 0.5$), the observed variations in the b -parameter result from systematic and random effects not properly accounted for (see the Introduction, items 1-3). Therefore, all attempts to connect β -value variability with various physical parameters and conditions are eventually bound to fail. However, studying the b - or β -values in local and regional earthquake catalogs may still be useful, especially if such investigations are needed to evaluate seismic hazard and seismicity forecasts that would be prospectively tested with the same catalogs. In addition, when seismic activity or earthquake productivity level is calculated for large earthquakes, the regular β -estimates can be used.

If the hypothesis about the β -value constancy is correct, we should investigate spatial changes in the corner moment that seem to explain major modifications in the deformation processes in solids. Bird *et al.* (2009) showed that the relation between relative plate velocity and seismicity is non-linear for several types of plate boundaries. Can the change in corner moment explain some of these non-linearities?

If the hypothesis that the power-law exponent is a universal constant and the corner moment is variable is correct, then it would provide a new theoretical approach to features of earthquake occurrence and account for the transition from brittle to plastic deformation.

More extensive investigation of corner moment behavior may afford new insight into regular earthquake occurrence and recently discovered slow deformation and seismic tremor events at the brittle-plastic crust boundary. As often happens in complex systems, new laws and features may be found to illuminate the transition from brittle fracture to plastic flow.

Acknowledgments

I am grateful to Dave Jackson, Paul Davis, Peter Bird, Karin Dahmen, and especially to Jeremy Zechar for useful discussion and suggestions. I thank Kathleen Jackson for significant improvements in the text. The author appreciates support from the National Science Foundation through grant EAR-0711515, as well as from the Southern California Earthquake Center (SCEC). SCEC is funded by NSF Cooperative Agreement EAR-0529922 and USGS Cooperative Agreement 07HQAG0008. Publication 0000, SCEC.

REFERENCES

- Abramowitz, M. and Stegun, I. A., (Eds.), 1972. *Handbook of Mathematical Functions*, Dover, NY, pp. 1046.
- Antsyferov, M. S., Y. Y. Kagan, and N. G. Antsyferova, 1971a. Seismoacoustical studies of aftershocks, in: *Tashkent Earthquake, April 26, 1966*, Fan, Tashkent, pp. 154-163 (in Russian); (ТАШКЕНТСКОЕ ЗЕМЛЕТРЯСЕНИЕ 26 апреля 1966 года), see http://moho.ess.ucla.edu/~kagan/Tashkent_1966.pdf
- Antsyferov, M. S., N. G. Antsyferova, and Y. Y. Kagan, 1971b. *Seismoacoustical Studies and the Problem of Prediction of Dynamic Events*, Nauka, Moscow, pp. 136 (in Russian); (Анцыферов, М. С., Н. Г. Анцыферова, и Я. Я. Каган, 1971. Сейсмоакустические Исследования и Проблема Прогноза Динамических Явлений), pp. 115-123 contain a report on these measurements, see http://moho.ess.ucla.edu/~kagan/Tashkent_AAK.pdf
- Beroza, G. C., and S. Ide, 2009. Deep Tremors and Slow Quakes, *Science*, **324**(5930), 1025-1026, DOI: 10.1126/science.1171231.
- Bird, P., and Y. Y. Kagan, 2004. Plate-tectonic analysis of shallow seismicity: apparent boundary width, beta, corner magnitude, coupled lithosphere thickness, and coupling in seven tectonic settings, *Bull. Seismol. Soc. Amer.*, **94**(6), 2380-2399 (plus electronic supplement).
- Bird, P., Y. Y. Kagan, D. D. Jackson, F. P. Schoenberg, and M. J. Werner, 2009. Linear and Nonlinear Relations Between Relative Plate Velocity and Seismicity, *Bull. Seismol. Soc. Amer.*, **99**(6), 3097-3113 (plus electronic supplement).
- Boettcher, M., and T. H. Jordan, 2004. Earthquake scaling relations for mid-ocean ridge transform faults, *J. Geophys. Res.*, **109**(B12), Art. No. B12302, doi:10.1029/2004JB003110.

- Boettcher, M. S., A. McGarr, and M. Johnston, 2009. Extension of Gutenberg-Richter distribution to $M_W - 1.3$, no lower limit in sight, *Geophys. Res. Lett.*, **36**, L10307, doi: 10.1029/2009GL038080.
- Clauset, A., Shalizi, C. R., and Newman, M. E. J., 2009. Power-law distributions in empirical data, *SIAM Rev.*, **51**, 661-703.
- Csikor, F. F., C. Motz, D. Weygand, M. Zaiser, S. Zapperi, 2007. Dislocation Avalanches, Strain Bursts, and the Problem of Plastic Forming at the Micrometer Scale, *Science*, **318**(5848), 251-254.
- Dahmen, K. A., Y. Ben-Zion, and J. T. Uhl, 2009. Micromechanical Model for Deformation in Solids with Universal Predictions for Stress-Strain Curves and Slip Avalanches, *Phys. Rev. Lett.*, **102**(17), Article Number: 175501.
- Dimiduk, D. M., Woodward, C., LeSar, R., Uchic, M. D., 2006. Scale-Free Intermittent Flow in Crystal Plasticity, *Science*, **312**, 1188-1190.
- Dziewonski, A. M., Chou, T.-A., and Woodhouse, J. H., 1981. Determination of earthquake source parameters from waveform data for studies of global and regional seismicity, *J. Geophys. Res.*, **86**, 2825-2852.
- Dziewonski, A. M., and Woodhouse, J. H., 1983. An experiment in systematic study of global seismicity: centroid-moment tensor solutions for 201 moderate and large earthquakes of 1981, *J. Geophys. Res.*, **88**, 3247-3271.
- Ekström, G., 2007. Global Seismicity: Results from Systematic Waveform Analyses, 1976-2005, in *Treatise on Geophysics*, **4**(4.16), ed. H. Kanamori, pp. 473-481.
- Ekström, G., A. M. Dziewonski, N. N. Maternovskaya and M. Nettles, 2005. Global seismicity of 2003: Centroid-moment-tensor solutions for 1087 earthquakes, *Phys. Earth planet. Inter.*, **148**(2-4), 327-351.

- Enescu, B., J. Mori, M. Miyazawa, and Y. Kano, 2009. Omori-Utsu Law c -Values Associated with Recent Moderate Earthquakes in Japan, *Bull. Seismol. Soc. Amer.*, **99**(2A), 884-891.
- Feller, W., 1966. *An Introduction to Probability Theory and its Applications*, **2**, J. Wiley, New York, 626 pp.
- Frohlich, C. and Davis, S.D., 1999. How well constrained are well-constrained T, B, and P axes in moment tensor catalogs?, *J. geophys. Res.*, **104**, 4901-4910.
- Frohlich, C. and L. R. Wetzel, 2007. Comparison of seismic moment release rates along different types of plate boundaries, *Geophys. J. Int.*, **171**(2), 909-920, doi: 10.1111/j.1365-246X.2007.03550.x
- Geist, E.L., and T. Parsons, 2005. Triggering of tsunamigenic aftershocks from large strike-slip earthquakes: Analysis of the November 2000 New Ireland earthquake sequence, *Geochemistry Geophysics Geosystems*, **6**, Article Number: Q10005.
- Gutenberg, B. and Richter, C.F., 1944. Frequency of earthquakes in California, *Bull. seism. Soc. Am.*, **34**, 185-188.
- Harris, T. E., 1963. *The Theory of Branching Processes*, Springer, New York, 230 pp.
- Hiramatsu, Y., T. Watanabe, and K. Obara, 2008. Deep low-frequency tremors as a proxy for slip monitoring at plate interface, *Geophys. Res. Lett.*, **35**, L13304, doi:10.1029/2008GL034342.
- Kagan, Y. Y., 1982. Stochastic model of earthquake fault geometry, *Geophys. J. Roy. astr. Soc.*, **71**(3), 659-691.
- Kagan, Y. Y., 1991a. Seismic moment distribution, *Geophys. J. Int.*, **106**(1), 123-134.
- Kagan, Y. Y., 1991b. Likelihood analysis of earthquake catalogues, *Geophys. J. Int.*, **106**(1), 135-148.

- Kagan, Y. Y., 1992. On the geometry of an earthquake fault system, *Phys. Earth Planet. Inter.*, **71**(1-2), 15-35.
- Kagan, Y. Y., 1999. Universality of the seismic moment-frequency relation, *Pure Appl. Geoph.*, **155**(2-4), 537-573.
- Kagan, Y. Y., 2000. Temporal correlations of earthquake focal mechanisms, *Geophys. J. Int.*, **143**(3), 881-897.
- Kagan, Y. Y., 2002a. Seismic moment distribution revisited: I. Statistical results, *Geophys. J. Int.*, **148**(3), 520-541.
- Kagan, Y. Y., 2002b. Aftershock zone scaling, *Bull. Seismol. Soc. Amer.*, **92**(2), 641-655.
- Kagan, Y. Y., 2003. Accuracy of modern global earthquake catalogs, *Phys. Earth Planet. Inter. (PEPI)*, **135**(2-3), 173-209.
- Kagan, Y. Y., 2004. Short-term properties of earthquake catalogs and models of earthquake source, *Bull. Seismol. Soc. Amer.*, **94**(4), 1207-1228.
- Kagan, Y. Y., 2007. Earthquake spatial distribution: the correlation dimension, *Geophys. J. Int.*, **168**(3), 1175-1194.
- Kagan, Y. Y., 2009. On the geometric complexity of earthquake focal zone and fault systems: A statistical study, *Phys. Earth Planet. Inter.*, **173**(3-4), 254-268, DOI: 10.1016/j.pepi.2009.01.006.
- Kagan, Y. Y., 2010. Statistical distributions of earthquake numbers: consequence of branching process, *Geophys. J. Int.*, **180**(3), 1313-1328. doi: 10.1111/j.1365-246X.2009.04487.x
- Kagan, Y. Y., P. Bird, and D. D. Jackson, 2010. Earthquake Patterns in Diverse Tectonic Zones of the Globe, *Pure Appl. Geoph. (The Frank Evison Volume)*, **167**(6/7), in press, DOI: 10.1007/s00024-010-0075-3, http://scec.ess.ucla.edu/~ykagan/globe_index.html .

- Kagan, Y. Y., and L. Knopoff, 1981. Stochastic synthesis of earthquake catalogs, *J. Geophys. Res.*, **86**(B4), 2853-2862.
- Kanamori, H., 1977. The energy release in great earthquakes, *J. Geophys. Res.*, **82**, 2981-2987.
- Miguel, M.-C., A. Vespignani, S. Zapperi, J. Weiss and J.-R. Grasso, 2001. Intermittent dislocation flow in viscoplastic deformation, *Nature*, **410**, 667-671, doi:10.1038/35070524.
- Molchan, G. M., and V. M. Podgaetskaya, 1973. Parameters of global seismicity, I, in: Keilis-Borok, V. I., (ed.), *Computational Seismology*, **6**, Nauka, Moscow, 44-66, (in Russian).
- Okal, E. A., and B. A. Romanowicz, 1994. On the variation of b -values with earthquake size, *Phys. Earth Planet. Inter.*, **87**, 55-76.
- Otter, R., 1949. The Multiplicative Process, *Annals Math. Statistics*, **20**(2), 206-224.
- Park, S.C., and J. Mori, 2007. Triggering of earthquakes during the 2000 Papua New Guinea earthquake sequence, *J. Geophys. Res.*, **112**(B3), Article Number: B03302.
- Perez-Campos, X., S.K. Singh, and G.C. Beroza, 2003. Reconciling teleseismic and regional estimates of seismic energy, *Bull. Seismol. Soc. Amer.*, **93**(5), 2123-2130.
- Rhoades, D. A., 1996. Estimation of the Gutenberg-Richter relation allowing for individual earthquake magnitude uncertainties, *Tectonophysics*, **258**, 71-83.
- Rhoades, D. A., 1997. Estimation of attenuation relations for strong-motion data allowing for individual earthquake magnitude uncertainties, *Bull. Seismol. Soc. Amer.*, **87**(6), 1674-1678.
- Rhoades, D.A., and Dowrick, D.J., 2000. Effects of magnitude uncertainties on seismic hazard estimates, Proceedings of the 12th World Conference on Earthquake Engineering, Auckland, New Zealand, 30th January - 4th February 2000, Paper No. 1179. New

- Zealand Society for Earthquake Engineering, Upper Hutt, New Zealand, *Bull. N.Z. Soc. Earthqu. Eng.*, **33**(3).
- Richeton, T., J. Weiss and F. Louchet, 2005. Breakdown of avalanche critical behaviour in polycrystalline plasticity, *Nature Materials*, **4**, 465-469.
- Schorlemmer D., S. Wiemer, and M. Wyss, 2005. Variations in earthquake-size distribution across different stress regimes, *Nature*, **437**, 539-542.
- Schwartz, S.Y., and J.M. Rokosky, 2007. Slow slip events and seismic tremor at circum-pacific subduction zones, *Reviews Geophysics*, **45**(3), Art. No. RG3004
- Shelly, D. R., G. C. Beroza, and S. Ide, 2007. Non-volcanic tremor and low frequency earthquake swarms, *Nature*, **446**, 305-307.
- Thomson Scientific/ISI <http://www.isinet.com/> ISI Web of Science, 2006. The Thomson Corporation, Thomson Reuters' Web of Science <http://portal.isiknowledge.com/portal.cgi> (last accessed July 2009).
- Tinti, S., and F. Mulargia, 1985. Effects of magnitude uncertainties on estimating the parameters in the Gutenberg-Richter frequency-magnitude law, *Bull. Seismol. Soc. Amer.*, **75**, 1681-1697.
- Vere-Jones, D., 1976. A branching model for crack propagation, *Pure Appl. Geophys.* (PAGEOPH), **114**, 711-725.
- Vere-Jones, D., 1977. Statistical theories of crack propagation, *Math. Geol.*, **9**, 455-481.
- Vere-Jones, D., 1988. Statistical aspects of the analysis of historical earthquake catalogues, in: C. Margottini, ed., *Historical Seismicity of Central-Eastern Mediterranean Region*, pp. 271-295.
- Weiss, J., and D. Marsan, 2003. Three-dimensional mapping of dislocation avalanches: clustering and space/time coupling, *Science*, **299**, 89-92.

- Wolfram, S., 1999. *The Mathematica Book*, 4th ed., Champaign, IL, Wolfram Media, Cambridge, New York, Cambridge University Press, pp. 1470.
- Zaiser, M., 2006. Scale invariance in plastic flow of crystalline solids, *Advances Physics*, **55**(1-2), 185-245.
- Zaiser, M., and P. Moretti, 2005. Fluctuation phenomena in crystal plasticity – a continuum model, *J. Statistical Mechanics*, doi:10.1088/1742-5468/2005/08/P08004.
- Zaiser, M., Schwerdtfeger, J., Schneider, A. S., Frick, C. P., Clark, B. G., Gruber, P. A. and Arzt, E., 2008. Strain bursts in plastically deforming molybdenum micro- and nanopillars, *Philosophical Magazine*, **88**(30), 3861-3874.
- Zhuang, J., Y. Ogata, and D. Vere-Jones, 2002. Stochastic declustering of space-time earthquake occurrences, *J. Amer. Statist. Assoc. (JASA)*, **97**, 369-380.
- Zhuang, J. C., Y. Ogata, and D. Vere-Jones, 2004. Analyzing earthquake clustering features by using stochastic reconstruction, *J. Geophys. Res.*, **109**(B5), Art. No. B05301.

Table 1: Parameter values for relative errors.

Approximation	n	c_0	c_1	c_2	ρ	σ
CMT 1977-2008, $m_t = 5.6$						
Linear	8508	-1.20	-0.352		-0.47	0.274
Quadratic	8508	-1.23	-0.513	0.198	-0.47	0.267
CMT 1982-2008, $m_t = 5.4$						
Linear	11600	-1.21	-0.447		-0.57	0.274
Quadratic	11600	-1.26	-0.537	0.208	-0.57	0.266

n , the number of $m \geq m_t$ events; for c_0 , c_1 , and c_2 see (11);

ρ , correlation coefficient; σ , standard deviation of fit.

For the linear approximation, the c_2 parameter is shown as a dash.

Table 2: The β -values for various subdivisions of CMT catalog.

#	Earthquakes	$m_t = 5.6$		$m_t = 5.8$	
		β	Eq. #	β	Eq. #
1	2	3	4	5	6
1.	Global	0.6773	7369	0.6820	5450
2.	Global declustered	0.6480	5841	0.6568	4498
3.	Global aftershocks included	0.6229	5605	0.6366	4358
4.	Trenches (Subduction zones)	0.6463	4805	0.6507	3223

Shallow earthquakes in 1977-2008 ($m_t = 5.8$) and 1982-2008 ($m_t = 5.6$) CMT catalog.

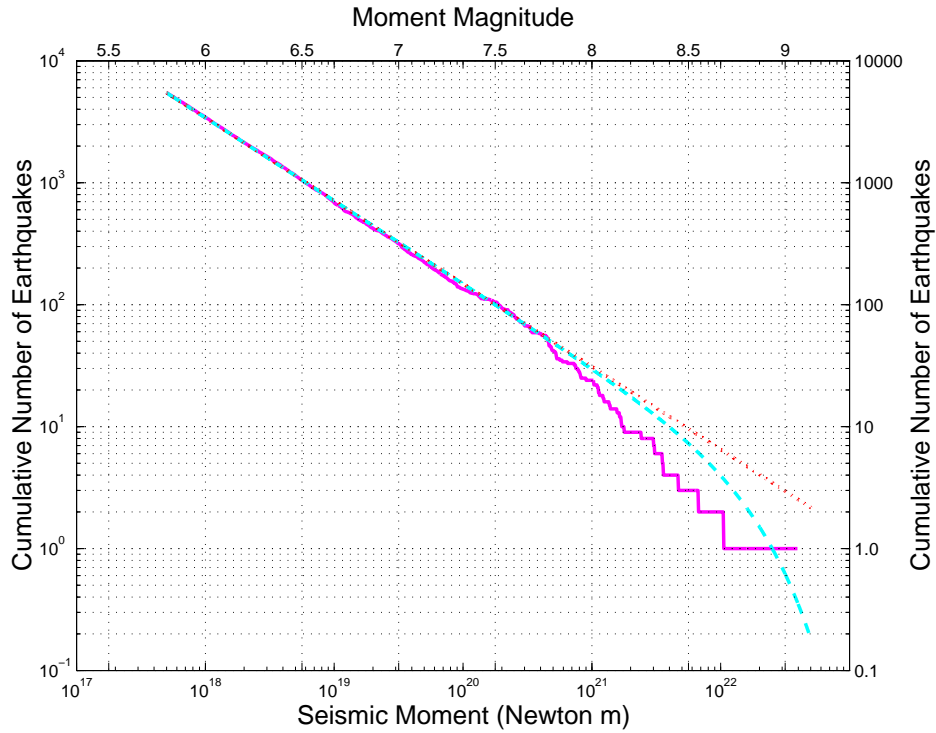


Figure 1:

Number of earthquakes with moment (M) larger than or equal to M as a function of M for the shallow earthquakes in the CMT catalog during 1977–2008, moment threshold $M_t = 10^{17.7}$ Nm ($m_t = 5.8$), the total number of events 5450. Power-law approximation (equivalent to Gutenberg-Richter law) is shown by dotted line. Dashed line shows tapered Gutenberg-Richter distribution: the G-R law restricted at large seismic moments by an exponential taper with the corner magnitude $m_c = 8.9$. The slope of the linear part of the curve corresponds to $\beta = 0.68$.

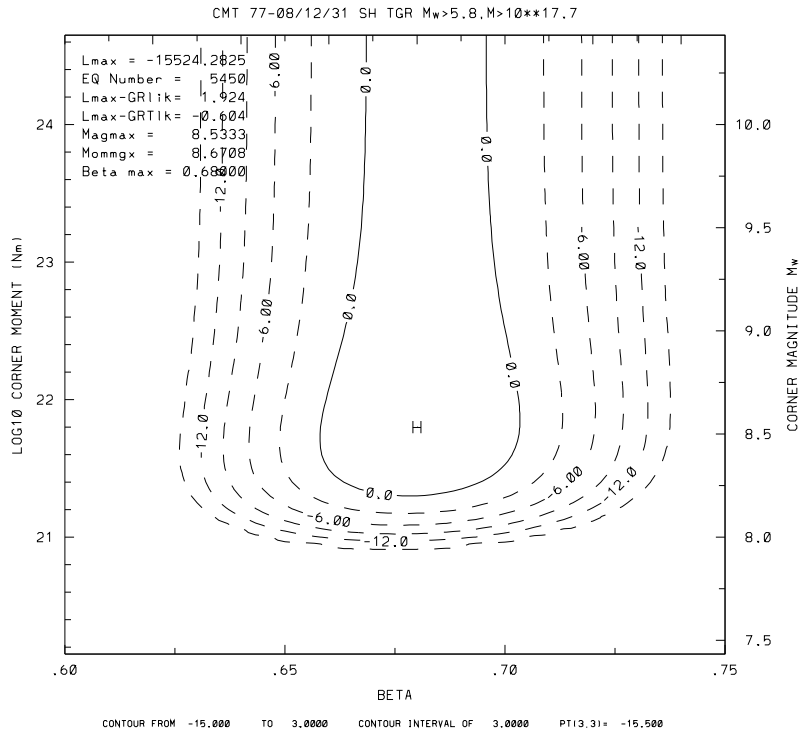


Figure 2:

Log-likelihood maps for the distribution of scalar seismic moment of earthquakes: The CMT catalog time span is 1977 January 1 – 2008 December 31; the seismic moment cutoff is $10^{17.7}$ Nm ($m_t = 5.8$); the number of events is 5450. *H*-sign on the plot denotes the maximum likelihood estimate of the parameters of interest.

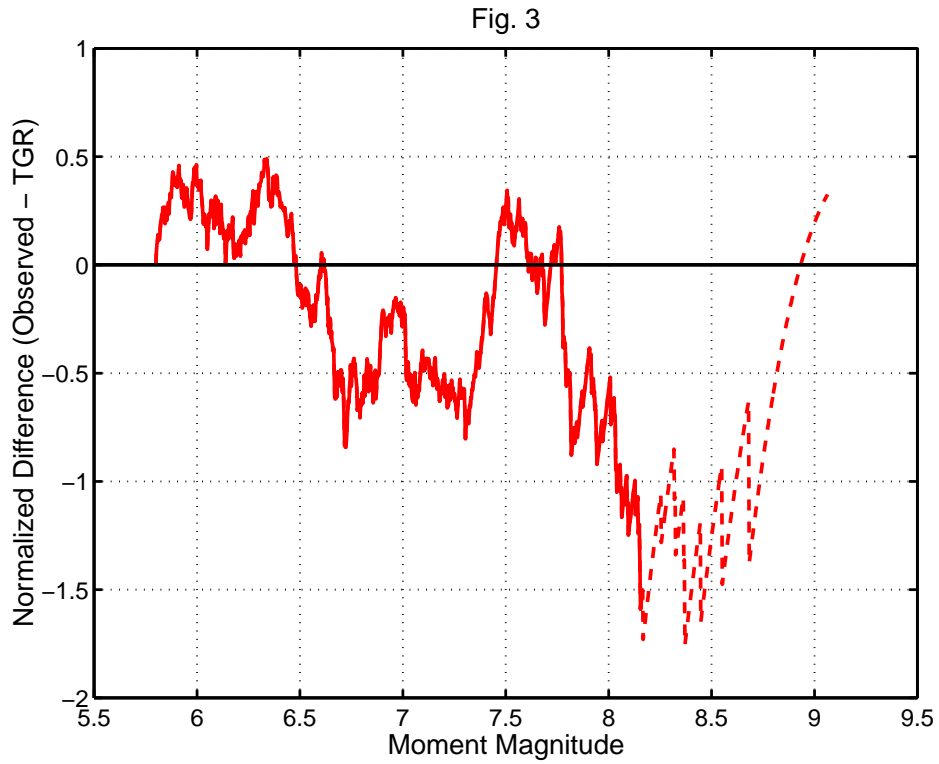


Figure 3:

Difference between observed magnitude-frequency relation and its approximation by tapered G-R law (see Fig. 1). CMT catalog 1977–2008, magnitude threshold $m_t = 5.8$. The dashed line indicates where the difference is based on fewer than 10 events.

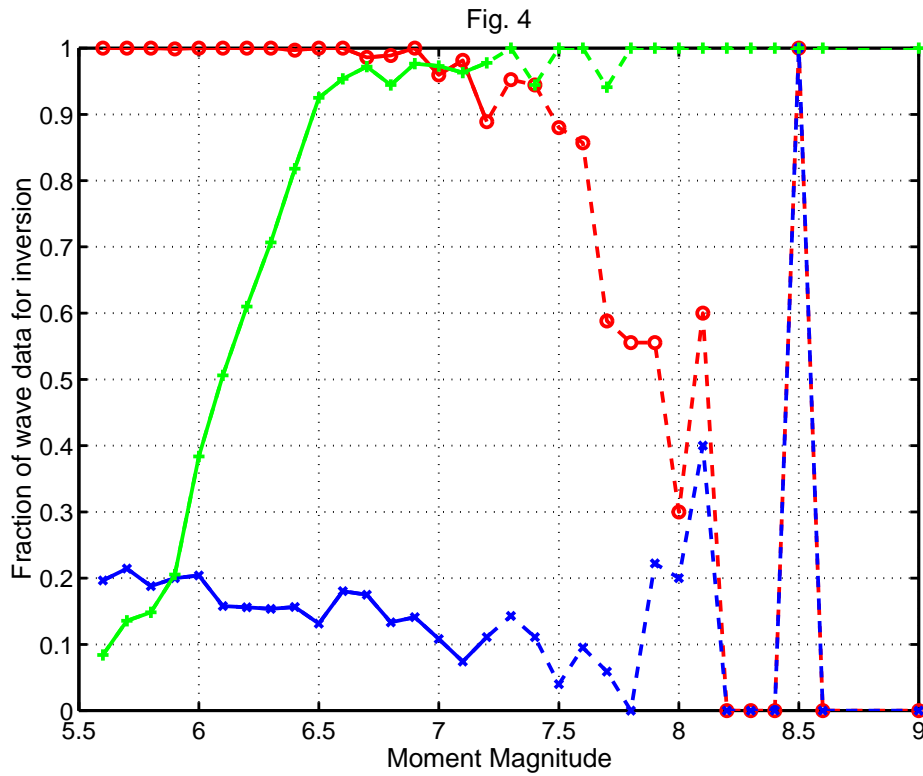


Figure 4:

Percentage of moment tensor solutions inversion of CMT data based on different waves: body waves – red line, circles; surface waves – blue line, x-marks; mantle waves – green line, pluses. Dashed lines are for data with fewer than 10 earthquakes in the 0.1 magnitude interval.

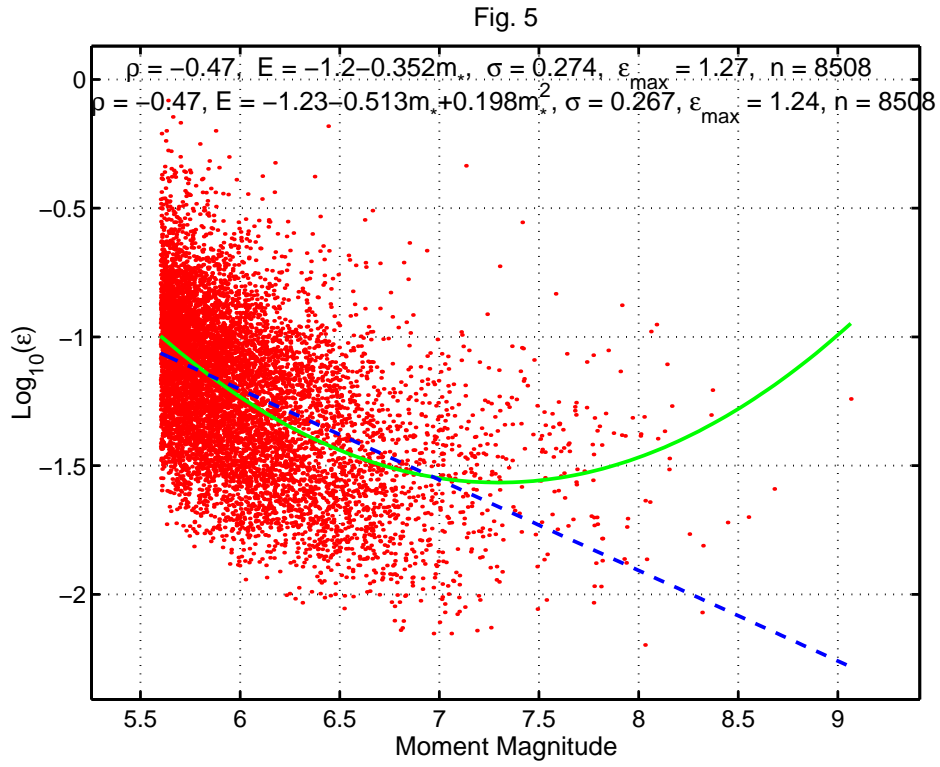


Figure 5:

Relative error ϵ versus moment magnitude for shallow earthquakes $m_t = 5.6$ in the 1977–2008 CMT catalog. The curves show two approximations: linear and quadratic fits.

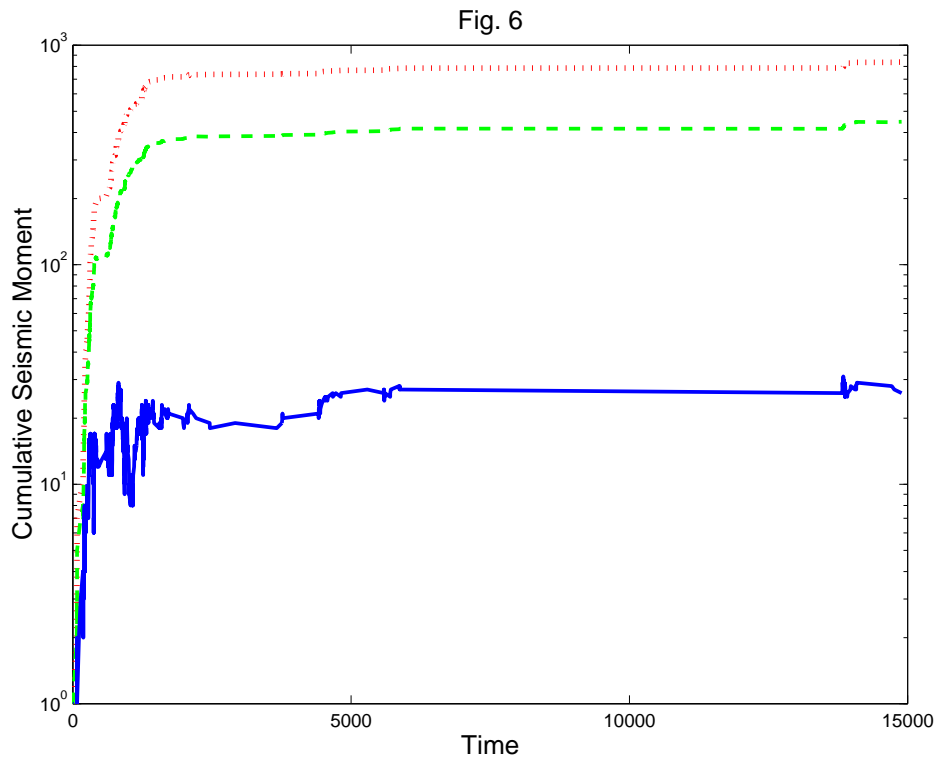


Figure 6:

Simulated source-time functions in a critical branching process. Red dotted line – positive number addition ($p = 1.0$). Green dashed line – unequal positive/negative number addition (random walk with a drift, $p = 0.75$). Blue solid line – equal positive/negative number addition $p = 0.5$ (random walk).

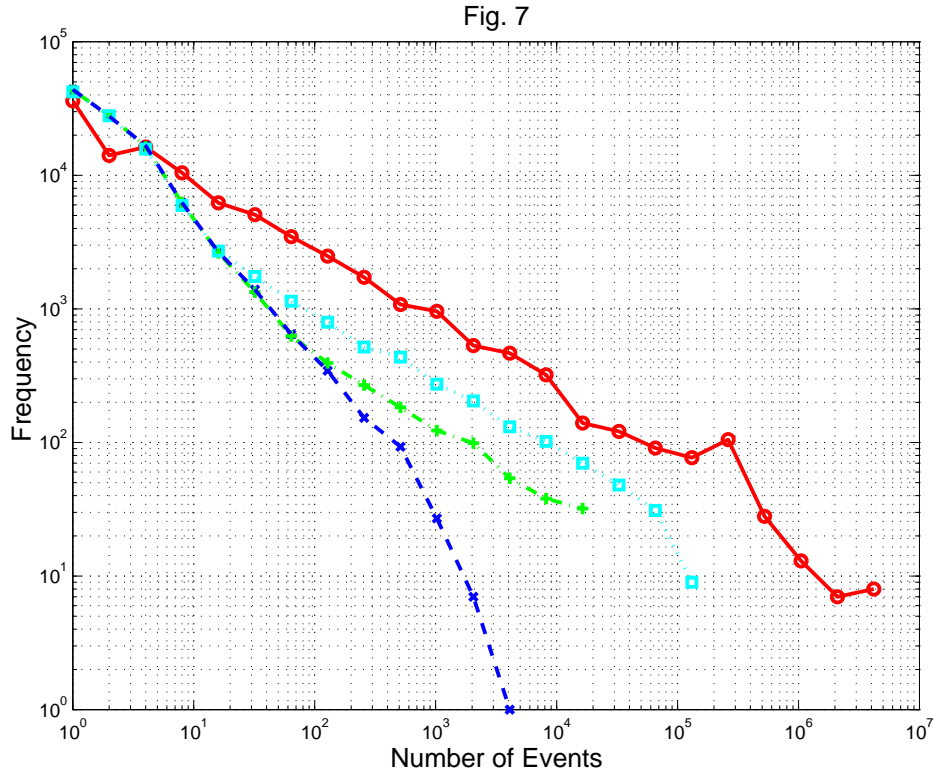


Figure 7:

Distribution of event numbers in a critical branching process. Red line, circles – positive deterministic number addition ($p = 1.0$). Blue line, x-marks – equal positive/negative number addition $p = 0.5$ (random walk). Green line, pluses – unequal positive/negative number addition (random walk with a drift, $p = 0.51$). Cyan lines, squares – unequal positive/negative number addition (random walk with a drift, $p = 0.55$).

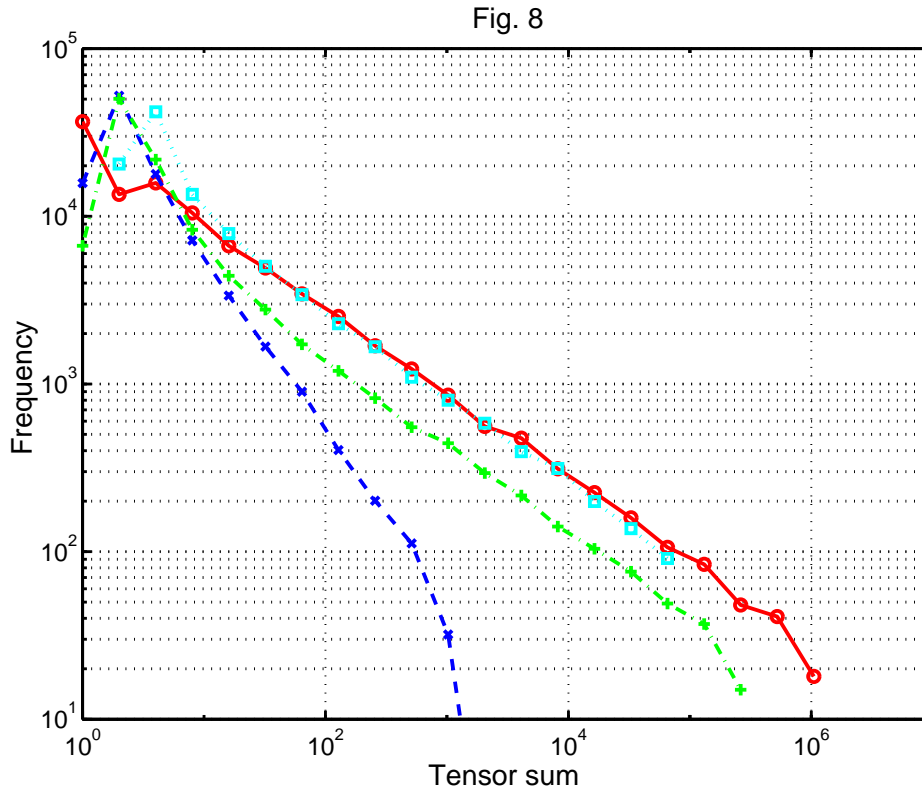


Figure 8:

Frequency plot of tensor sum norm in a critical branching process. Red line, circles – tensor sum with no rotation, the 3-D rotation angle, $\Phi = 0^\circ$. Blue dashed line – random rotation ($\Phi = 120^\circ$). Green line, pluses – limited random rotation, $\Phi = 80^\circ$. Cyan line, squares – limited random rotation, $\Phi = 30^\circ$.

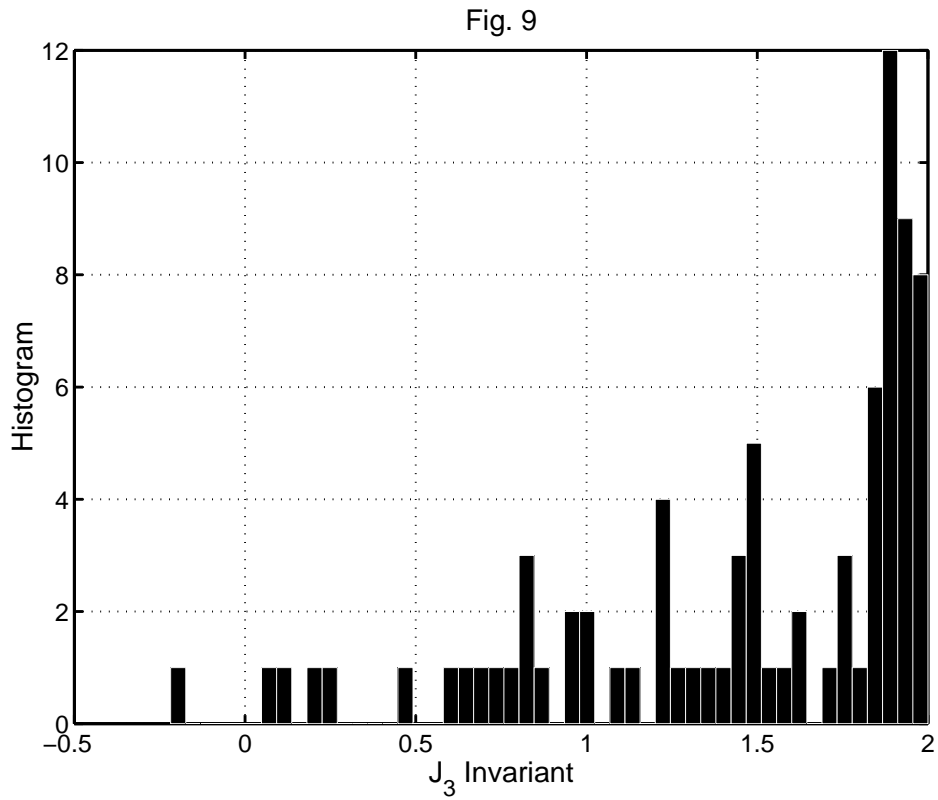


Figure 9:

Frequency plot of correlation tensor invariant (tensor dot-product) for $m7.5$ mainshocks and sum of their immediate aftershocks in 1977-2008 CMT catalog. Average $\overline{J_3} = 1.458$, its standard error $\sigma_J = 0.5535$.

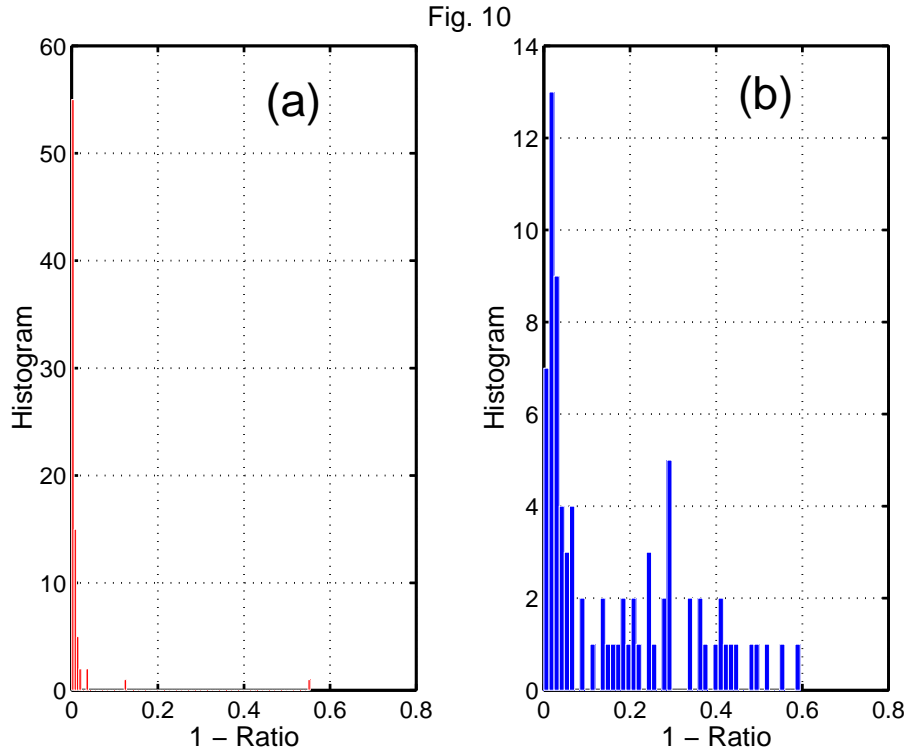


Figure 10:

Frequency plot of tensor/scalar sum ratio for $m7.5$ mainshocks and immediate aftershocks in 1977-2008 CMT catalog: (a) Unnormalized sum - average $\overline{(1 - R)} = 0.0128$, its standard error $\sigma = 0.0627$. (b) Normalized sum - average $\overline{(1 - R)} = 0.1642$, its standard error $\sigma = 0.1639$.

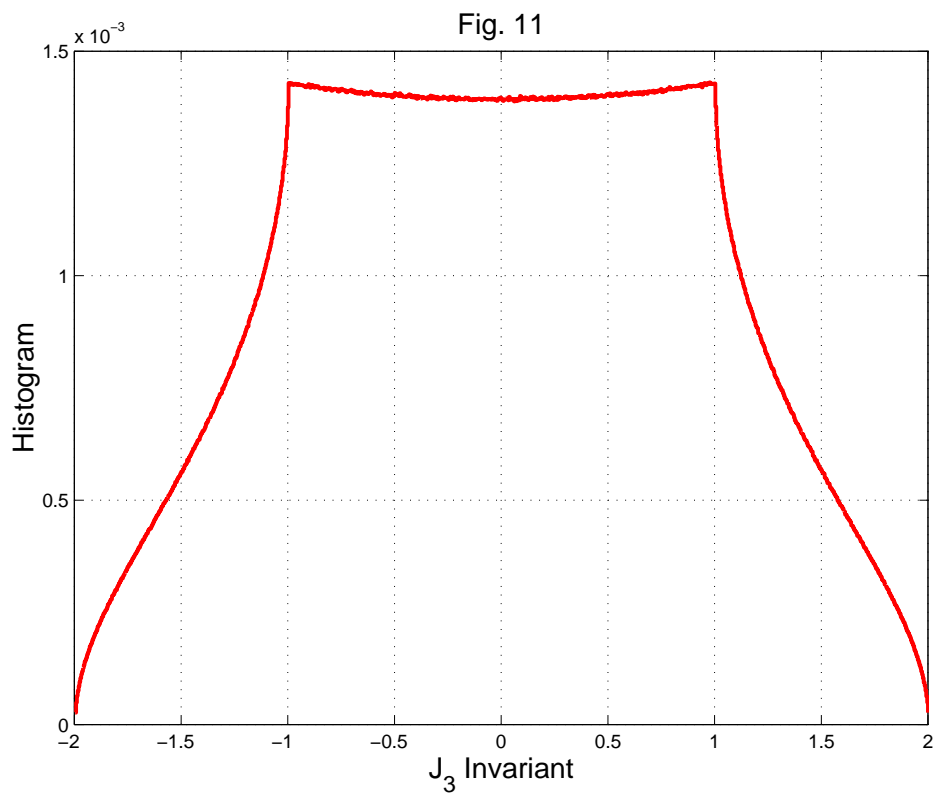


Figure 11:

Frequency plot of tensor dot-product invariant for random rotation of double-couple sources.

Average $\overline{J_3} = 0$, its standard error $\sigma_J = 0.8945$.

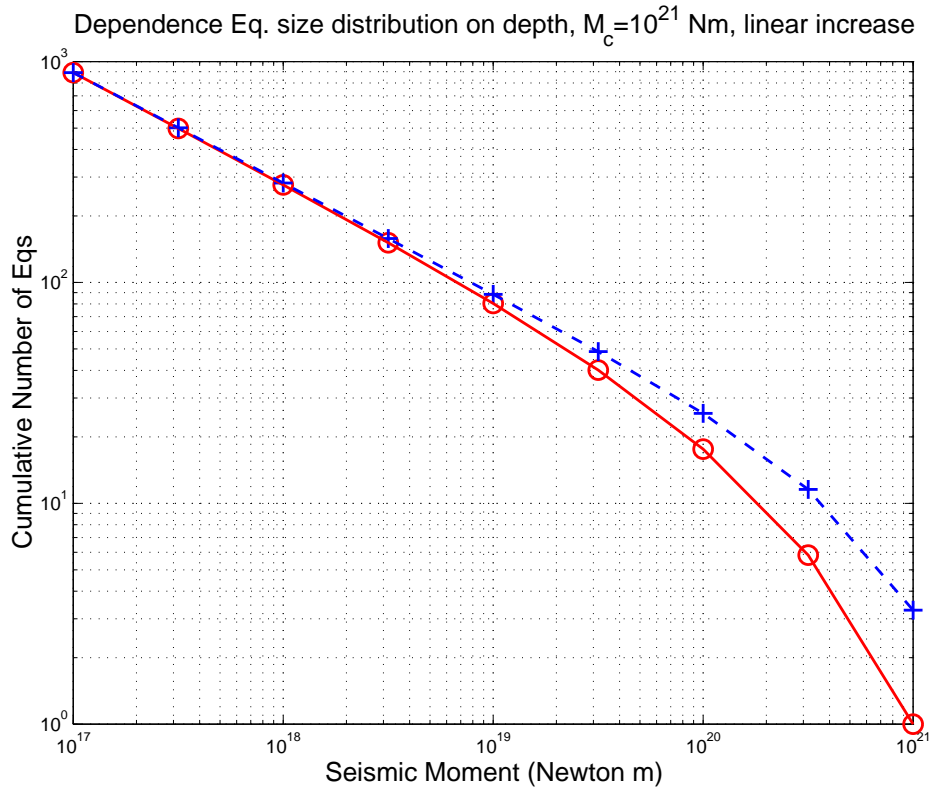


Figure 12:

Two theoretical moment-frequency curves: the number of earthquakes with moment (M) larger than or equal to M as a function of M , moment threshold $M_t = 10^{17.0}$ Nm ($m_t = 5.33$). Dashed line shows tapered Gutenberg-Richter distribution: the G-R law restricted at large seismic moments by an exponential taper with the corner moment $10^{21.0}$ Nm ($m_c = 8.0$). The slope of the linear part of the curve corresponds to $\beta = 0.50$. The solid line is a plot for Eq. 19, with a half-width of a fault, $L = 10$ km, and $C = 1.0$. The curves are normalized so that the solid line has an ordinate 1.0 at the right-hand end.